ORIGINAL RESEARCH

Changes of Lipopolysaccharide-Induced Acute Kidney and Liver Injuries in Rats Based on Metabolomics Analysis

Huan Gao [iD][1]
Tao Yang[2]
Xuan Chen[3]
Yanqing Song[1]

[1]Department of Pharmacy, The First Hospital of Jilin University, Changchun, 130021, People's Republic of China; [2]Houde Food Co., Ltd, Liaoyuan, 136200, People's Republic of China; [3]Department of Neurosurgery, The First Hospital of Jilin University, Changchun, 130021, People's Republic of China

Background: The bacterial endotoxin lipopolysaccharide (LPS) was the classic inducer to establish many inflammatory disease models, especially multiple organ injury. Evidences indicated that the mechanism that causes inflammation response is not just related to cytokine release. The main aim of this study was to better elucidate the possible links between metabolic changes and the pathogenesis of LPS-induced acute liver and kidney in order to understand the mechanisms and screening therapeutic targets for developing early diagnostic strategies and treatments.

Methods: An experimental rat model was established by intraperitoneal injection of 10 mg/kg LPS. An untargeted metabolomics analysis of the serum in the LPS and control groups was carried out using ultra-performance liquid chromatography/quadrupole time-of-flight mass spectrometry (UPLC/QTOF-MS). LPS-induced pathological damage in the lungs, liver, kidneys, and colon was observed, along with changes in biochemical indexes, indicating that there was a severe inflammatory response in many organs after administration of LPS for 8 h. Principal component analysis (PCA) and partial least squares-discriminant analysis (PLS-DA) showed distinct separation in the serum metabolite profiles between the LPS and control groups, indicating significant changes in endogenous metabolites.

Results: The untargeted metabolomics analysis showed that there were 127 significantly different serum metabolites and 53 altered pathways after LPS administration, including pathways related to the metabolism of D-glutamine and D-glutamate, taurine and hypotaurine, beta-alanine, glutathione, and butanoate, which are involved in the inflammatory response, oxidative stress, and amino acid metabolism.

Conclusion: The study suggested that LPS-induced acute liver and kidney injury mainly involves inflammatory response, oxidative stress, and protein synthesis, finally causing multi-organ damage. Correcting the disturbances to the metabolites and metabolic pathways may help to prevent and/or treat LPS-induced acute liver and kidney damage.

Keywords: untargeted metabolomics, LPS, acute kidney injury, acute liver injury, amino acid metabolism

Increasing studies have reported that the bacterial endotoxin lipopolysaccharide (LPS) could impact levels of inflammatory mediators, playing an important role in the development of systemic inflammatory response which may trigger sepsis and be linked to acute kidney and liver injury. Thus, LPS has been administered to animals to create reliable experimental models that provide mechanistic insights into how cells and organs respond to inflammation; then these models have been extensively employed to assess strategies to prevent or attenuate systemic

Correspondence: Yanqing Song
Department of Pharmacy, The First Hospital of Jilin University, Changchun, 130021, People's Republic of China
Tel +86 431 88782482
Email songyanq@jlu.edu.cn

1807

inflammatory response or multiple organ failure.[1,2] Responses in organs and tissues to endotoxemia are closely associated with alterations in metabolism and catabolic signals. Metabolites, including lipids, amino acids and glucose, have been identified during the process of inflammatory process in plasma.[3,4] There is a dual directional regulation between metabolite levels and inflammatory defenses,[5] and understanding the alterations in the serum metabolome during injuries is critical for making and directing more precise and personalized therapeutic intervention. Therefore, comprehensive metabolomics-based evaluation of LPS-induced acute kidney and liver injury is necessary.

Metabolomics analysis can be used to monitor disturbances in endogenous small-molecule metabolites in cells, tissues, and biofluids of the body in response to a toxicant or other environmental change, and it is a viable approach for continued discovery around the pathophysiology, diagnosis and prognosis and provides a greater level of biochemical detail and insight than other systems' biology methods.[6] Ultra-high-performance liquid chromatography coupled to quadrupole time-of-flight mass spectrometry (UPLC-Q/TOF-MS) and gas chromatography-mass spectrometry (GC-MS) have been used to quantitatively analyze various metabolites in biological samples, rapidly and effectively separating and identifying the individual compounds, which are more sensitive than nuclear magnetic resonance (NMR). Furthermore, UPLC-MS is commonly used for "untargeted" metabolomics due to its broad range of different types of metabolites.[7]

In this study, changes in the plasma metabolites of a rat model of LPS-induced acute kidney and liver injuries were assessed using UPLC-Q/TOF-MS, along with assessing the pathological signs in the main organs and serum. This allowed the identification of altered metabolites and metabolic pathways, to better understand the pathogenesis of LPS-induced acute kidney and liver injuries and to provide new insights into the development of early diagnostic strategies and treatments.

Materials and Methods
Chemicals and Reagents

LPS from *Escherichia coli* 055:B5 was purchased from Sigma-Aldrich (USA). Commercial enzyme-linked immunosorbent assay (ELISA) kits to assess the levels of the cytokines tumor necrosis factor (TNF)-α and interleukin (IL)-6 and a terminal deoxynucleotidyl transferase dUTP nick end labeling (TUNEL) kit were obtained from R&D Systems (USA). Radioimmunoprecipitation assay (RIPA) lysis buffer and superoxide dismutase (SOD), catalase (CAT), and malondialdehyde (MDA) assay kits were purchased from Beyotime Co. Ltd. (China). Acetonitrile and methanol (high-performance liquid chromatography [HPLC] grade) were obtained from Thermo Fisher Scientific (USA). Ultra-pure distilled water was prepared using a Milli-Q purification system (Millipore Corp., USA). All other reagents (analytical grade) were obtained from Sigma-Aldrich (USA).

Animals

A total of 20 Sprague–Dawley rats (male, 200–220 g) were randomly divided into the LPS model group and the control group (n=10 per group). The rats were obtained from the Center of Experimental Animals of Baiqiuen Medical College of Jilin University (Jilin, China). The experiment was approved by the Jilin University Animal Care and Use Ethics Committee (protocol number 2019–239) and performed in accordance with the National Institutes of Health guide for the care and use of laboratory animals. After acclimatization for 1 week, the rats in the LPS group were intraperitoneally injected with 10 mg/kg LPS (dissolved in normal saline) which was based on earlier reports and the rats in the control group were intraperitoneally injected with an equivalent amount of normal saline.[8,9] After 8 h, the rats were anesthetized using chloral hydrate, and then blood was collected by direct puncture of the abdominal aorta. The blood was then centrifuged at $3000 \times g$ to prepare a serum sample. Organ tissues were collected and divided into two parts; one part was fixed in 4% formaldehyde, and the other was frozen in liquid N_2. All serum and tissue samples were stored at −80 until biochemical analysis.

Metabolomics Analysis

Each serum sample was thawed at 4°C, and 100 μL of each sample was transferred to a tube. About 400 μL methanol was added to the tube and vortexed for 1 min. After centrifuging at 4°C for 10 min at 12,000 rpm, the supernatant was collected and transferred to another tube to concentrate it using a vacuum concentrator. Next, 150 μL 2-chlorobenzalanine in 80% methanol solution was added and a 0.22-μm membrane was used to filter the samples for LC-MS. To prepare the quality control (QC) samples, 20 μL was obtained from each tube.[10,11]

Chromatographic separation was performed using an UltiMate 3000 System (Thermo Fisher Scientific) equipped with an ACQUITY UPLC HSS T3 column (150×2.1 mm, 1.8 μm; Waters, USA) maintained at 40°C. The temperature of the autosampler was 8°C. Gradient elution of the analytes was carried out using 0.1% formic acid in water (C) and in acetonitrile (D) in the positive ion mode, or 5 mM ammonium formate in water (A) and acetonitrile (B) in the negative ion mode at a flow rate of 0.25 mL/min. After equilibration, 2 μL of each sample was injected. An increasing linear gradient of solvent B (negative mode) or solvent D (positive mode) (v/v) was used as follows: 0–1 min, 2% B/D; 1–9 min, 2–50% B/D; 9–12 min, 50–98% B/D; 12–13.5 min, 98% B/D; 13.5–14 min, 98–2% B/D; and 14–17 min, 2% B (negative mode) or 14–20 min, 2% D (positive mode).

Electrospray ionization (ESI)-multistage mass spectrometry (MSn) experiments were performed using a Q Exactive mass spectrometer (Thermo Fisher Scientific) with a spray voltage of 3.8 and −2.5 kV in the positive and negative ion mode, respectively. The sheath gas and auxiliary gas were set at 30 and 10 arbitrary units, respectively. The capillary temperature was 325°C. The analyzer scanned over a mass range of m/z 81–1000 for a full scan at a mass resolution of 70,000, with data-dependent acquisition of

higher-energy collision dissociation (HCD) MS/MS spectra. The normalized collision energy was 30 eV. Dynamic exclusion was implemented to remove some of the unnecessary information in the MS/MS spectra.[12] The metabolomics study workflow is shown in Figure 1. A random QC sample was inserted into the sequence of samples after every set of five real samples. The samples were analyzed in one batch to eliminate system errors. The compounds or metabolites were selected and confirmed according to retention time (RT), exact molecular weight (m/z), mass spectra, and peak intensity (PI). A principal component analysis (PCA) was then carried out to verify the quality of the data and the stability and repeatability of the analytical method.

The raw UPLC-MS/MS data were converted into mzXML format by Proteowizard software (v3.0.8789). The data were analyzed using XCMS package of R language (v3.3.2) for peaks identification, peaks filtration and peaks alignment. The major parameters were bw=2, ppm=15, peakwidth=c(5, 30), mzwid=0.015, mzdiff=0.01, method= "centWave". Information concluding Mass to charge ratio (m/z), retention time (rt) and peak intensity were collected for further study. Batch normalization of peak area was applied.[13] Then the data were used to search several qualitative metabolomics databases,
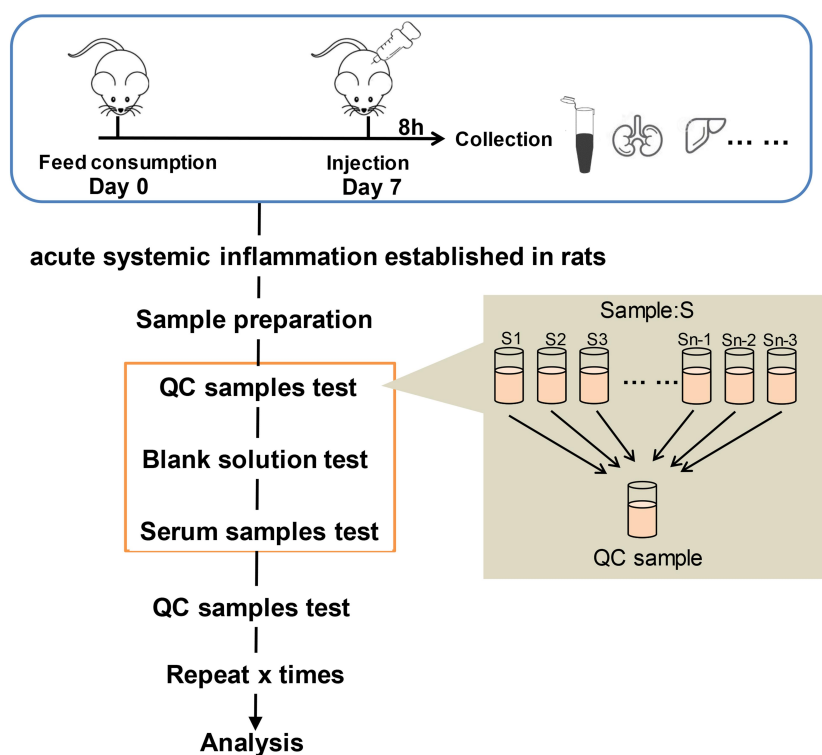

Figure 1 Metabolomics study workflow.

comprising the mzCloud database (www.mzcloud.org), the Human Metabolome Database (www.hmdb.ca), METLIN (metlin.scripps.edu), MoNA (mona. fiehnlab.ucdavis.edu), and MassBank (www.massbank.jp).

To identify candidate biomarkers (ie, the differential serum metabolites between the LPS and control groups), the following criteria were used: Variable Importance in Projection (VIP) value ≥1 and Student's t-test P value ≤0.05. PCA and partial least squares-discriminant analysis (PLS-DA) were conducted using R language.[14] A metabolite correlation analysis was also conducted based on Pearson's correlation coefficients, and R language was used to visualize the results in a chord diagram.

A pathway enrichment analysis of the differential metabolites was conducted, using MetaboAnalyst (www. metaboanalyst.ca) to map the metabolites to pathways in the Kyoto Encyclopedia of Genes and Genomes (KEGG) database (www.kegg.jp) in order to identify the altered metabolic pathways.[15]

ELISAs

The levels of the inflammatory factors tumor necrosis factor (TNF)-α and interleukin (IL)-6 in the serum were assessed using the ELISA kits (R&D Systems) according to the manufacturer's instructions.

Determination of SOD, CAT, and MDA Levels in Serum

SOD, CAT, and MDA are biomarkers of oxidative stress, representing the degree of damage and antioxidant abilities of organs or cells. Using the assay kits (Beyotime, China), the samples were processed according to the manufacturer's instructions. The protein in each sample was quantified. After incubation, the absorbance value was assessed using a microplate reader (EL808; Bio-TEK Instruments, USA).

Histopathological Analysis

Kidney, lung, liver, colon, hippocampus, and cerebral cortex tissues were fixed in 4% formaldehyde immediately after obtaining them from the rats. The tissues were then subjected to an alcohol gradient, embedded in paraffin, and sectioned at a thickness of 5 μm. Histopathological examination was performed after hematoxylin and eosin (H&E) staining. Images were visualized using a light microscope (Nikon Eclipse TS200; Nikon Corp., Japan) at 100×, 200×, or 400× magnification.

TUNEL Assays

The paraffin-embedded tissues were sectioned at a thickness of 5 μm in the coronal plane using a freezing microtome (CM1950; Leica, Wetzlar, Germany). TUNEL assays (Roche, Germany) were conducted according to the manufacturer's instructions. Images were visualized using a microscope (Nikon Eclipse TS200; Nikon Corp., Japan) at 200×magnification.

Complete Blood Cell Count Analysis

Whole blood was collected at the time of euthanasia via direct puncture of the abdominal aorta and stored in tubes pre-filled with ethylenediaminetetraacetic acid (EDTA). The analysis was performed using an ABC Vet Animal Blood Counter (Scil Animal Care Company, Gurnee, IL, USA) according to the manufacturer's instructions. The red blood cell (RBC), white blood cell (WBC), monocyte, neutrophil, and lymphocyte counts were assessed.[16]

Statistical Analysis

The experiments were designed following the standard approach to ensure adequate sample sizes for reliable statistical analysis.[17,18] The data are presented as mean ± standard error of the mean (SEM). The data were analyzed using GraphPad Prism 5 (GraphPad Software). Statistical significance was analyzed by means of two-tailed Student's t-test or analysis of variance (ANOVA). A p-value <0.05 was considered statistically significant.

Results
Effects of LPS on Blood Counts

The RBC, WBC, monocyte, neutrophil, and lymphocyte counts were measured in whole blood from rats. The WBC count was significantly decreased in the LPS group compared to the control group (Figure 2A). Differential WBC analysis (Figure 2B–E) revealed that LPS notably increased the percentages of circulating monocytes, neutrophils, and lymphocytes, which may lead to acute systemic inflammation. LPS had no effect on the RBC count.

Effects of LPS on Cytokine, SOD, CAT, and MDA Levels in Serum

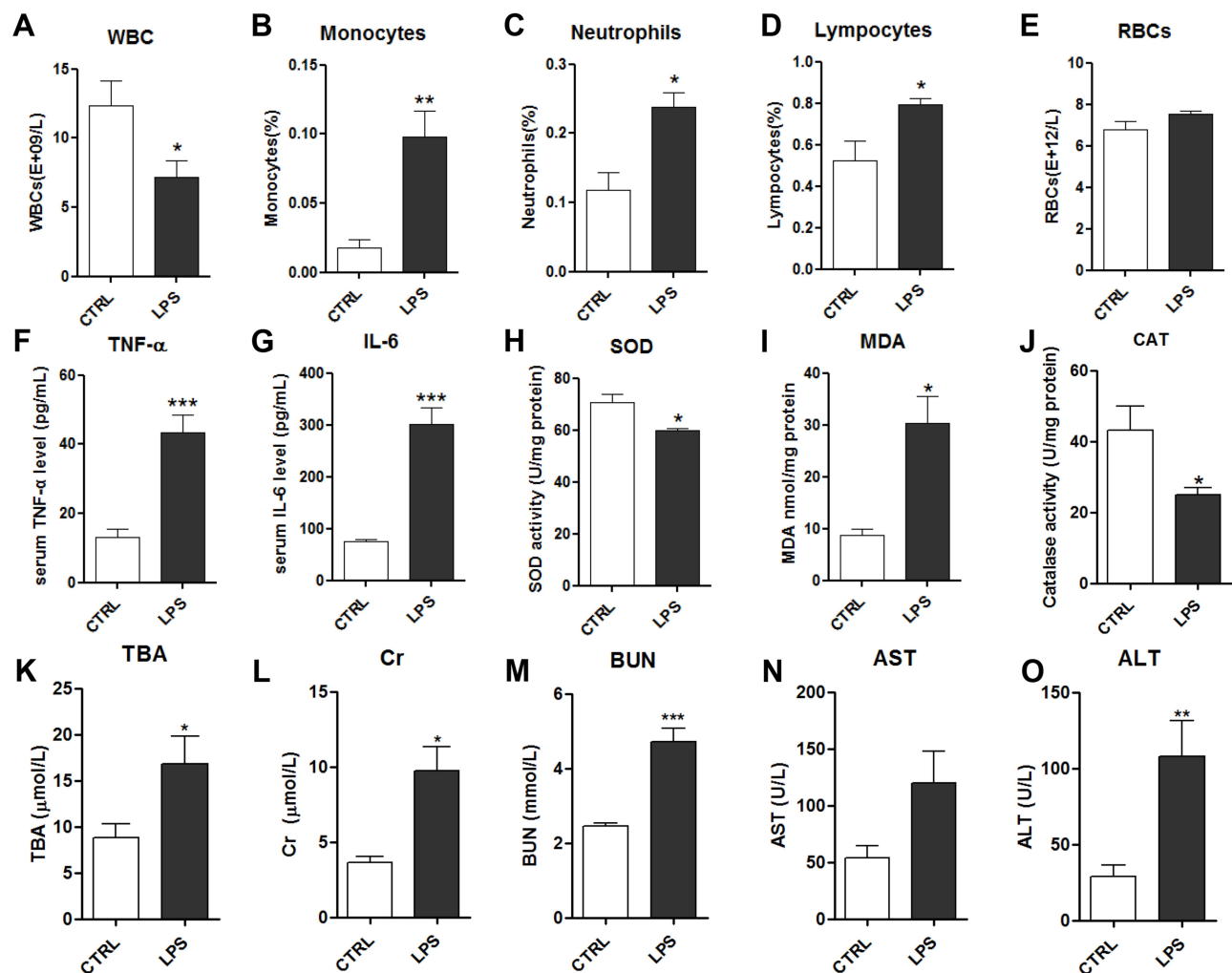The inflammatory cytokines TNF-α and IL-6 were measured in the serum using ELISAs. TNF-α and

Figure 2 Effects of LPS on serum biochemical indicators: white blood cells (WBCs) (**A**), monocytes (**B**), neutrophils (**C**), lymphocytes (**D**) and red blood cells (RBCs) (**E**); serum levels of TNF-α (**F**) and IL-6 (**G**); serum levels of the oxidative stress factors superoxide dismutase (SOD) (**H**), malondialdehyde (MDA) (**I**), and catalase (CAT) (**J**); and kidney and liver function indicators: total bile acids (TBA) (**K**), creatine (Cr) (**L**), blood urea nitrogen (BUN) (**M**), aspartate transaminase (AST) (**N**) and alanine transaminase (ALT) (**O**).
Notes: Data are expressed as mean ± SEM (n=10 per group). *$p<0.05$, **$p<0.01$, ***$p<0.001$ vs control group.

IL-6 were significantly increased in the LPS group compared to the control group (Figure 2F–G). As oxidative stress is highly associated with inflammatory injury, biochemical methods were used to assess multiple factors, comprising the MDA level and the activities of the antioxidant enzymes SOD and CAT. The antioxidant enzymes SOD and CAT were significantly decreased in the LPS group compared to the control group, while MDA was significantly increased in the LPS group (Figure 2H–J). These results suggested that 10 mg/kg LPS could induce inflammation and oxidative stress in rats after 8 h, which may disrupt the function of tissues and organs.

Effects of LPS on the Kidney and Liver Function

To evaluate the effects of LPS on liver function, alanine transaminase (ALT) activity, aspartate transaminase (AST) activity, and total bile acid (TBA) levels in the serum were assessed. They were markedly increased in the LPS group compared to the control group, indicating that 10 mg/kg LPS caused considerable liver injury in the rats at 8 h (Figure 2K–O). Additionally, to evaluate the effects of LPS on kidney function, the mean serum blood urea nitrogen (BUN) and creatinine (Cr) levels were assessed, and they all increased after intraperitoneal injection of 10 mg/kg LPS (Figure 2L and M). Together, these data showed that

intraperitoneal injection of LPS induced severe systemic inflammation and caused kidney and liver damage.

Histopathological Evaluation in Multiple Tissues

H&E staining of liver sections revealed vacuolar degeneration, massive necrosis of hepatocytes, and severe inflammatory cell infiltration in the LPS group (Figure 3A–F). Additionally, there were more TUNEL-positive cells in the LPS group than in the control group (Figure 3G–L).

Regarding the kidney tissues, the epithelial cells of renal tubules showed vacuolar degeneration, damaged brush borders, and the presence of protein casts in the LPS group, unlike in the control group (Figure 3B). In addition, necrosis of tubular epithelial cells was observed in the LPS group. The results of TUNEL staining indicated apoptosis (Figure 3H), which suggests that renal pathological damage had already occurred at 8 h after LPS administration.

The lung tissues stained with H&E showed that the LPS-induced lung injury mainly involved a degree of inflammatory cell infiltration, destruction of alveoli, and thickened alveolar septa (Figure 3C). The damaged alveoli and apoptotic cells were clearer based on the TUNEL assays (Figure 3I).

Regarding the colon tissues, LPS administration led to inflammatory cell infiltration, partial mucosal epithelial damage, and missing goblet cells (Figure 3D). In contrast, the control rats had intact colon mucosal epithelia, along with normal colonic epithelial and goblet cells. There were also more TUNEL-positive cells in the LPS group than in the control group (Figure 3J), demonstrating that LPS caused severe injury in the colon.

Regarding H&E staining of the hippocampus tissues, the LPS rats had thinner cell layers and neuronal degeneration. In contrast, the control rats had normal morphology, with clear cell layers, nuclei, and nucleoli (Figure 3E). Regarding the cerebral cortex, LPS caused eosinophilic necrosis (Figure 3F). There were many TUNEL-positive apoptotic cells in the hippocampus and cerebral cortex tissues from LPS rats (Figure 3K and L).

Thus, LPS induced acute systemic inflammation, disrupting the normal function of multiple organs and damaging the liver, kidneys, colon, lungs, hippocampus, and cerebral cortex. Accordingly, the disease model was successfully established by 10 mg/kg LPS at 8 h after administration, and further analyses were carried out.

Validation of Metabolomics Data

The total ion chromatograms (TICs) in the positive and negative ion modes allowed differences to be observed visually (Figure 4A–D). By testing the QC samples
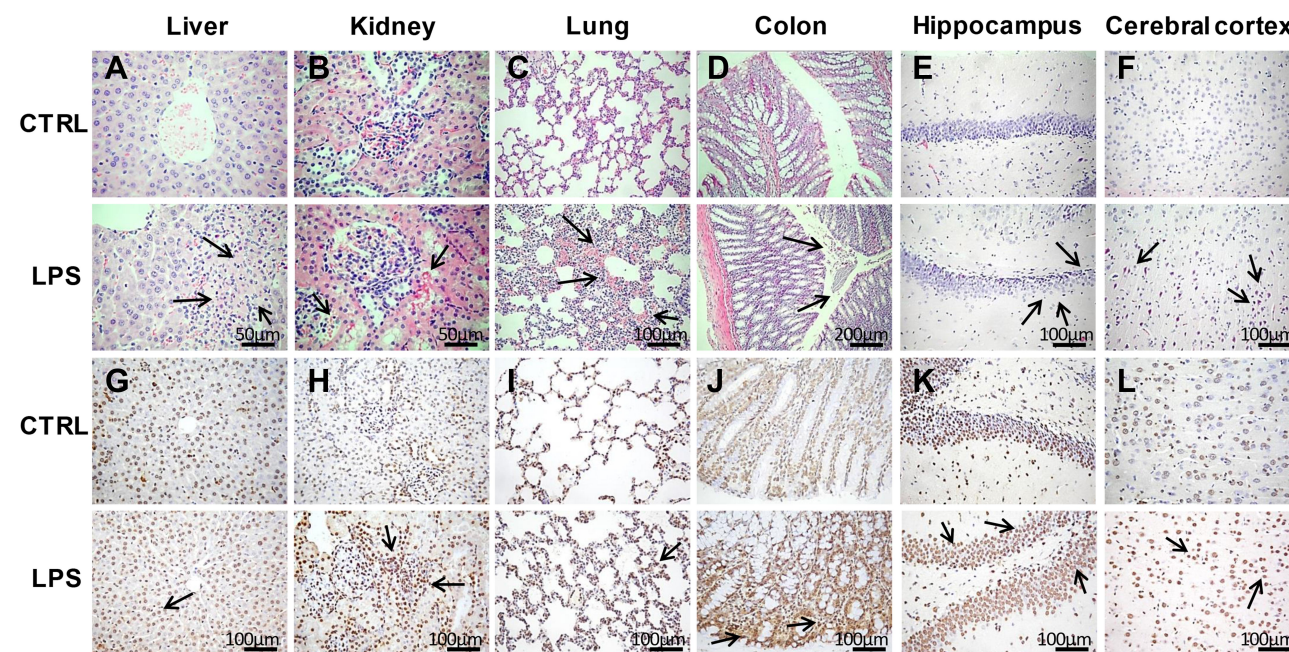
Figure 3 Histopathological analyses of tissues in the LPS and control groups. (**A–F**) Hematoxylin and eosin (H&E) staining of liver (400×), kidney (400×), lung (200×), colon (100×), hippocampus (200×), and cerebral cortex (200×) tissues in the LPS and control groups. (**G–L**) Terminal deoxynucleotidyl transferase dUTP nick end labeling (TUNEL) assays of liver, kidney, lung, colon, hippocampus, and cerebral cortex tissues (200×) in the LPS and control groups. The arrows point to the damage area.
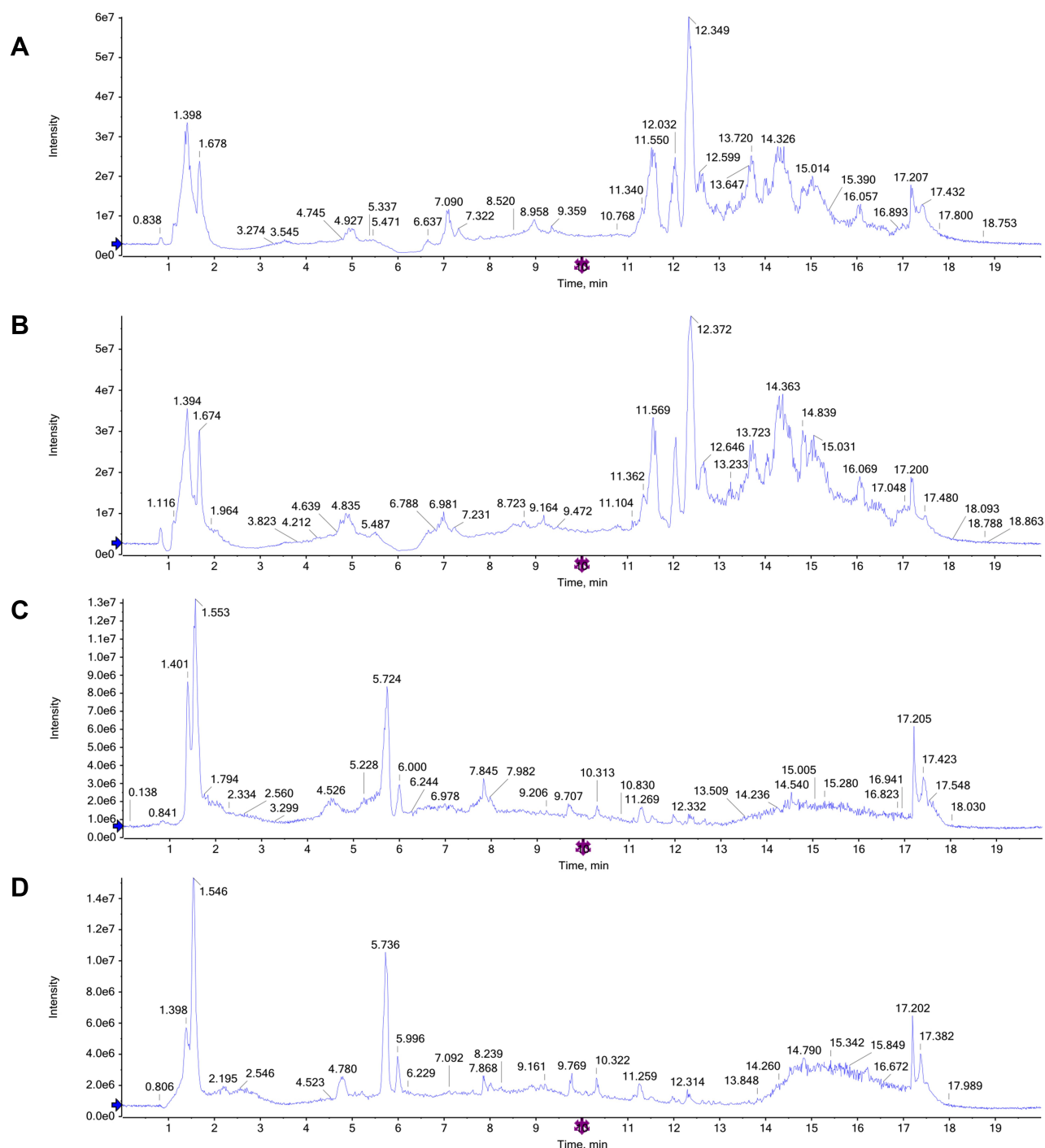
Figure 4 Representative total ion chromatograms (TICs) of serum samples subjected to (UPLC/QTOF-MS) in positive and negative ion modes. (**A** and **B**) TICs of CTRL group and LPS group in the positive ion modes; (**C** and **D**) TICs of CTRL group and LPS group in the negative ion modes.

along with the real samples, method repeatability and instrument precision were confirmed (relative standard deviation [RSD] <15%). In addition, the PCA score plots of the metabolic profiles of the QC samples indicated that the detection system was stable (in the Supplementary Material).

Multivariate Analysis of Metabolic Profiles

The PLS-DA score plots for the LPS and control groups indicated notable separation regarding both the negative and positive ion modes (Figure 5A–D). The PLS-DA model had a low risk of overfitting (R^2=0.92, Q^2=0.15 in the positive ion mode, and R^2=0.92, Q^2=0.1

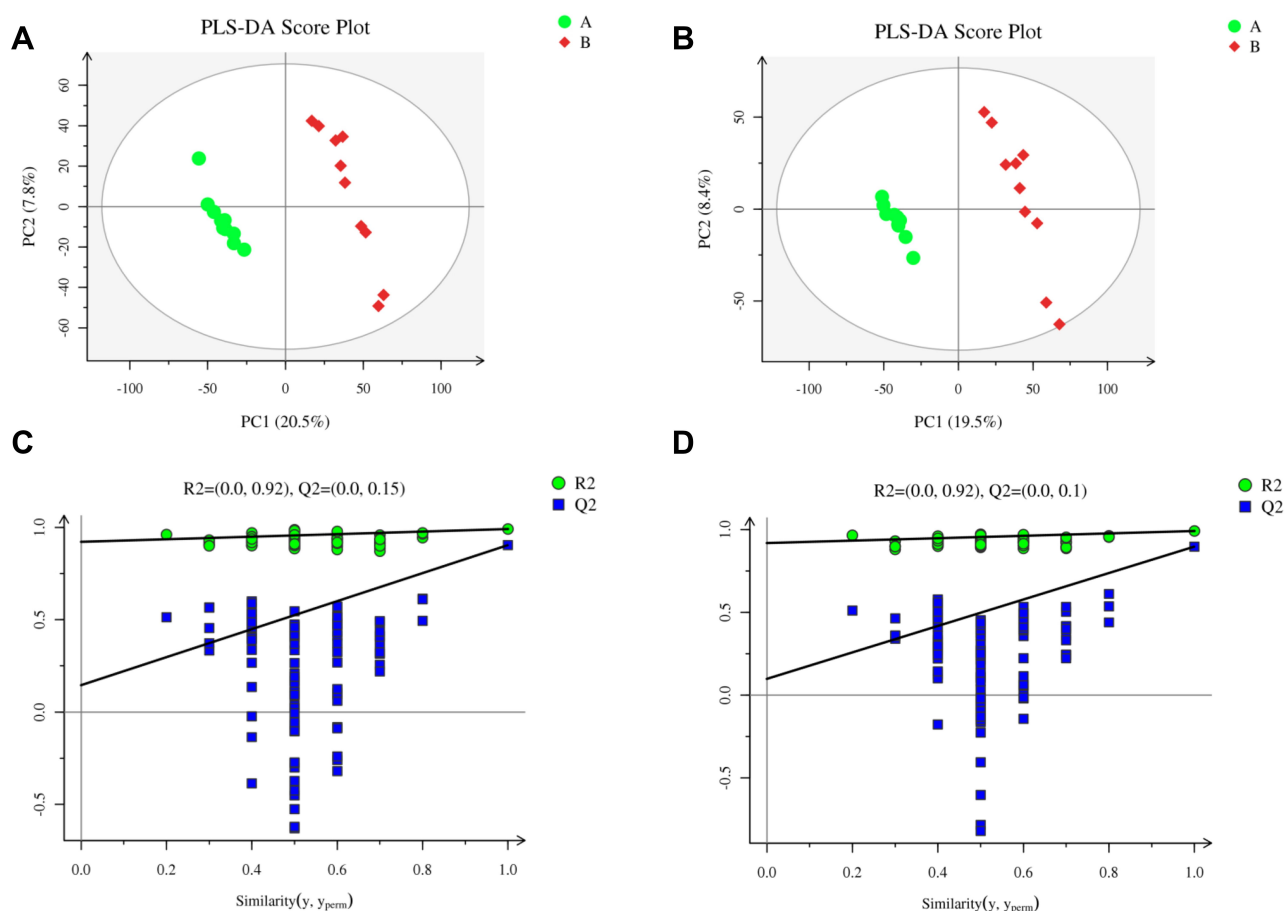**Figure 5** Metabolomics analysis of serum samples from rats in the LPS and control groups (n=10 per group) in the positive and negative ion modes. Partial least squares-discriminant analysis (PLS-DA) score plot in the (**A**) positive and (**B**) negative ion modes. Permutation test of PLS-DA model in the (**C**) positive and (**D**) negative ion modes.

in the negative ion mode), good fitness (R^2Y=0.991 in the positive ion mode, and R^2Y=0.991 in the negative ion mode), and good prediction (Q^2=0.904 in the positive ion mode, and Q^2=0.897 in the negative ion mode). These results indicate that the LPS-induced acute systemic inflammation model was successfully established.

Endogenous metabolites were picked if they met criteria related to multiple data processing methods (VIP ≥1 and P ≤0.05). Using R language and multiple metabolomics databases, the serum levels of 127 metabolites were significantly different between the LPS and control groups (Table 1). The 127 metabolites were divided into two groups; the levels of 59 metabolites decreased and the levels of 68 metabolites increased in the LPS group. The results of the correlation analysis were visualized using a chord diagram (Figure 6) and compounds belonging to the classes of amino acid, lipid, and carbohydrate were the most enriched in the changed endogenous metabolites.

Red indicates increased abundance and blue indicates decreased abundance.

Analysis of the Differential Metabolites and Pathways

Pathway enrichment and pathway topology analyses were performed to identify the pathways that were most relevant to the differential metabolites that had been identified as candidate biomarkers, as well as the network of the matched pathways. Totally, 53 pathways were relevant to the candidate biomarkers. Several of these may play critical roles in the occurrence and development of acute systemic inflammation, including the pathways related to the metabolism of D-glutamine and D-glutamate, linoleic acid, taurine and hypotaurine, beta-alanine, glutathione, and butanoate. A graph of the 10 most relevant pathways was constructed, with the log(P) values from the pathway enrichment analysis on the *y*-axis and the pathway impact values from the pathway topology analysis on the *x*-axis

Table I Identification of Serum Endogenous Metabolites During LPS-Induced Acute Systemic Inflammation

No.		RT	m/z	Mode	Metabolites	Formula	KEGG	Pathway	VIP	P	Fold Change CTRL/LPS	Tendency in Model Samples
1	Amino acid	85.52	147.04796	[M]-	L-Glutamic acid	C5H9NO4	C00025	1, 4, 7, 33, 50	2.1417	5.612E-08	2.3650	Down
2		92.35	104.10701	[M+H]+	Gamma-Aminobutyric acid	C4H9NO2	C00334	1, 7, 11	2.0993	5.699E-08	1.5024	Down
3		396.96	298.09602	[M+H]+	5-Methylthioadenosine	C11H15N5O3S	C00170	3	2.0409	4E-07	0.3102	Up
4		85.88	132.02873	[M-H]-	L-Aspartic acid	C4H7NO4	C00049	1, 20, 22	2.0384	1.292E-06	2.0208	Down
5		106.83	613.15095	[M+H]+	Oxidized glutathione	C20H32N6O12S2	C00127	4	2.0367	4.531E-07	3.6806	Down
6		391.91	206.08193	[M-H]-	N-Acetyl-L-phenylalline	C11H13NO3	C03519	9	1.9666	6.555E-06	0.2031	Up
7		95.63	288.0738	[M+H]+	Indoleglycerol phosphate	C11H14NO6P	C03506	5	1.9568	3.517E-06	2.7345	Down
8		102.83	116.07015	[M+H]+	L-Proline	C5H9NO2	C00148	7	1.8878	1.451E-05	1.5651	Down
9		93.86	239.01536	[M-H]-	L-Cystine	C6H12N2O4S2	C00491	3	1.8875	2.833E-05	0.3699	Up
10		219.24	136.07489	[M+H]+	2-Phenylacetamide	C8H9NO	C02505	9	1.8839	1.562E-05	1.3932	Down
11		709.51	117.05395	[M]-	Guanidoacetic acid	C3H7N3O2	C00581	7, 22	1.8622	4.282E-05	0.3102	Up
12		812.56	116.92614	[M-H]-	Methylmalonic acid	C4H6O4	C02170	16, 18, 43	1.8387	6.167E-05	0.2975	Up
13		463.66	219.11207	[M+H]+	N-Acetylserotonin	C12H14N2O2	C00978	13	1.8041	6.027E-05	5.0426	Down
14		84.31	188.05558	[M-H]-	N-Acetylglutamic acid	C7H11NO5	C00624	47	1.7666	0.00017	2.1637	Down
15		397.18	136.0616	[M]+	Phenylacetic acid	C8H8O2	C07086	9	1.6887	0.0002962	0.5972	Up
16		92.99	106.04999	[M+H]+	L-Serine	C3H7NO3	C00065	3, 22, 32	1.6002	0.0008134	1.4324	Down
17		418.32	198.11233	[M+H]+	Metanephrine	C10H15NO3	C05588	23	1.5776	0.0010297	0.3770	Up
18		839.83	101.07103	[M]+	1-Aminocyclopropanecarboxylic acid	C4H7NO2	C01234	3	1.5383	0.0015187	0.4098	Up
19		93.54	148.07961	[M]+	2,3-Dihydroxy-3-methylvalerate	C6H12O4	C06007	26	1.5335	0.0015901	0.6896	Up
20		320.58	173.0789	[M]+	2-Oxoarginine	C6H11N3O3	C03771	7, 29	1.5202	0.0018031	0.4542	Up
21		92.13	124.00605	[M-H]-	Taurine	C2H7NO3S	C00245	50, 53	1.5014	0.0027829	1.5417	Down
22		71.26	111.05538	[M+H]+	Imidazole-4-acetaldehyde	C5H6N2O	C05130	28	1.4950	0.0022704	1.9201	Down
23		196.33	166.05778	[M]+	D-Phenyllactic acid	C9H10O3	C05607	9	1.4933	0.0023051	2.3332	Down
24		336.58	246.1525	[M+H]+	Beta-Alanyl-L-arginine	C9H19N5O3	C05340	30	1.4840	0.0025047	0.4130	Up
25		154.62	247.13983	[M+H]+	D-Octopine	C9H18N4O4	C04137	7	1.4473	0.003436	2.9978	Down
26		93.62	147.07582	[M+H]+	L-Glutamine	C5H10N2O3	C00064	1, 2, 33	1.4442	0.0035253	0.7408	Up
27		93.52	90.055385	[M+H]+	Beta-Alanine	C3H7NO2	C00099	20, 30	1.4077	0.0047457	1.3380	Down
28		70.63	131.97461	[M]+	Glutaric acid	C5H8O4	C00489	35, 44	1.3731	0.006202	0.9227	Up
29		196.31	182.08095	[M+H]+	Beta-Tyrosine	C9H11NO3	C04368	23	1.3581	0.0069395	1.3754	Down
30		152.83	136.06155	[M]+	4-Hydroxyphenylacetaldehyde	C8H8O2	C03765	23	1.3544	0.0071325	0.7163	Up
31		150.66	136.95299	[M]+	2-Aminobenzoic acid	C7H7NO2	C00108	13	1.3477	0.0074936	0.7611	Up
32		326.52	177.10205	[M+H]+	5-Hydroxytryptamine	C10H12N2O	C00780	13	1.3426	0.0077805	1.6931	Down
33		102.76	154.01655	[M+H]+	3-Sulfinoalanine	C3H7NO4S	C00606	3, 50	1.3352	0.0082028	2.4910	Down

(*Continued*)

Table 1 (Continued).

No.		RT	m/z	Mode	Metabolites	Formula	KEGG	Pathway	VIP	P	Fold Change CTRL/LPS	Tendency in Model Samples
34		348.68	209.09192	[M+H]+	3-Anthraniloyl-L-alanine	C10H12N2O3	C00328	13	1.3330	0.0083362	0.6056	Up
35		102.36	427.09116	[M+H]+	S-Glutathionyl-L-cysteine	C13H22N4O8S2	C05526	3	1.3297	0.0085367	1.3485	Down
36		78.37	89.107679	[M+H]+	Putrescine	C4H12N2	C00134	4, 7, 29	1.3263	0.0087457	0.3685	Up
37		444.35	130.06486	[M-H]-	3-Methylindole	C9H9N	C08313	13	1.3236	0.0106792	0.4467	Up
38		181.61	130.04916	[M+H]+	Pyroglutamic acid	C5H7NO3	C01879	4	1.3064	0.0100556	1.3047	Down
39		451.31	191.08114	[M]+	2-Amino-3,7-dideoxy-D-threo-hept-6-ulosonic acid	C7H13NO5	C16850	5	1.2849	0.0116425	1.9810	Down
40		451.06	160.07442	[M+H]+	Indoleacetaldehyde	C10H9NO	C00637	13	1.2233	0.0173649	1.9142	Down
41		431.86	190.04945	[M+H]+	Kynurenic acid	C10H7NO3	C01717	13	1.2212	0.0175879	0.6294	Up
42		160.73	248.05441	[M-H2O-H]-	S-Ribosyl-L-homocysteine	C9H17NO6S	C03539	3	1.2138	0.021276	1.7743	Down
43		96.11	174.08755	[M-H]-	L-Citrulline	C6H13N3O3	C00327	47	1.1905	0.024337	0.6324	Up
44		787.66	105.06989	[M+H-H2O]+	2-Phenylethanol	C8H10O	C05853	9	1.1857	0.0218212	1.6524	Down
45		101.15	116.04561	[M]+	Glutarate semialdehyde	C5H8O3	C03273	35	1.1769	0.0229994	0.7723	Up
46		96.48	145.0493	[M]+	2-Oxoglutaramate	C5H7NO4	C00940	1	1.1653	0.0246083	1.3173	Down
47		230.53	305.09713	[M+H]+	N-Acetylaspartylglutamic acid	C11H16N2O8	C12270	1	1.1556	0.0260294	0.5559	Up
48		794.90	156.12007	[M]+	3-Indoleacetonitrile	C10H8N2	C02938	13	1.1492	0.0269884	1.2237	Down
49		132.43	166.05252	[M+H]+	L-Methionine S-oxide	C5H11NO3S	C02989	3	1.1051	0.0344715	1.3616	Down
50		76.92	120.98084	[M]+	L-Cysteine	C3H7NO2S	C00097	3, 20, 22, 50	1.1003	0.0353727	3.3363	Down
51		152.87	219.09713	[M+H]+	Gamma-Glutamylalanine	C7H11N2O5R	C03740	4	1.0870	0.0379579	0.5292	Down
52		111.67	155.04301	[M+H]+	Imidazole pyruvate	C6H6N2O3	C03277	28	1.0862	0.0381262	0.5728	Up
53		222.79	132.10128	[M+H]+	L-Isoleucine	C6H13NO2	C00407	43	1.0849	0.0383927	1.4439	Down
54		185.84	162.07566	[M+H]+	O-Acetyl-L-homoserine	C6H11NO4	C01077	3	1.0759	0.0402448	0.5791	Up
55		207.90	177.04056	[M]-	N-Formyl-L-methionine	C6H11NO3S	C03145	3	45	0.0456168	1.6241	Down
56		257.22	161.04418	[M+H]+	Oxoadipic acid	C6H8O5	C00322	8, 13	1.0535	0.0451565	0.4988	Up
57	Carbohydrate	76.28	146.02944	[M]+	Oxoglutaric acid	C5H6O5	C00026	6, 33, 35, 47, 50	1.9426	4.812E-06	2.6342	Down
58		84.08	117.01783	[M-H]-	Succinic acid	C4H6O4	C00042	1, 6, 11, 14	1.9358	1.199E-05	1.8537	Down
59		76.45	151.03491	[M+H]+	D-Ribose	C5H10O5	C00121	10, 22, 32	1.8615	2.339E-05	2.4030	Down
60		87.23	105.01774	[M-H]-	Glyceric acid	C3H6O4	C00258	32	1.7429	0.0002301	1.8800	Down
61		687.24	139.9865	[M]+	Acetylphosphate	C2H5O5P	C00227	14, 50	1.7397	0.0001532	3.6373	Down

No.	Category	RT	m/z	Adduct	Name	Formula	KEGG	Pathway	VIP	p-value	FC	Trend
62		84.16	259.02215	[M-H]-	Fructose 6-phosphate	C6H13O9P	C00085	45, 48	1.7231	0.000294	1.7743	Down
63		847.75	165.0766	[M+H]+	L-Fucose	C6H12O5	C00507	24	1.5687	0.0011267	0.8916	Up
64		580.84	181.0493	[M+H]+	D-Fructose	C6H12O6	C00095	24, 45, 48	1.5002	0.0021661	0.4046	Up
65		86.07	324.09389	[M-H]-	N-Glycolylneuraminic acid	C11H19NO10	C03410	51	1.4693	0.0036356	1.3034	Down
66		420.15	177.05451	[M+H]+	2-Hydroxy-3-oxoadipate	C6H8O6	C03217	32	1.4467	0.0034521	1.5977	Down
67		82.99	115.00212	[M-H]-	Maleic acid	C4H4O4	C01384	11, 23, 51	1.4185	0.0054211	1.3706	Down
68		85.78	194.03817	[M]-	D-Glucuronic Acid	C6H10O7	C00191	52	1.3863	0.0068905	0.4635	Up
69		97.55	181.07057	[M-H]-	Galactitol	C6H14O6	C01697	48	1.3828	0.0070679	1.6941	Down
70		84.58	289.03361	[M-H]-	Sedoheptulose 7-phosphate	C7H15O10P	C05382	10	1.3491	0.0089739	2.0111	Down
71		398.36	183.10128	[M+H]+	Mannitol	C6H14O6	C00392	24	1.3477	0.0074953	0.4008	Up
72		131.53	89.02275	[M-H]-	L-Lactic acid	C3H6O3	C00186	14, 18, 24	1.3014	0.0123705	0.4545	Up
73		447.22	102.09117	[M]+	Succinic acid semialdehyde	C4H6O3	C00232	1, 11, 17, 23	1.2481	0.0148418	1.6362	Down
74		416.39	164.07022	[M]+	L-Rhamnofuranose	C6H12O5	C02431	24	1.2473	0.0149114	1.6877	Down
75		153.00	179.04493	[M+H]+	Gluconolactone	C6H10O6	C00198	10	1.1577	0.0257119	0.5064	Up
76		76.89	102.97047	[M+H]+	2-Ketobutyric acid	C4H6O3	C00109	3, 18, 22, 26	1.1473	0.0272784	2.6591	Down
77		44.62	116.10698	[M]+	Fumaric acid	C4H4O4	C00122	11, 14, 23, 39, 47	1.1402	0.0283987	0.6892	Up
78		754.41	343.29421	[M+H]+	Sucrose	C12H22O11	C00089	45, 48	1.0393	0.0485209	1.5138	Down
79	Cofactors and Vitamins	299.22	168.06561	[M-H]-	Pyridoxine	C8H11NO3	C00314	17	1.8292	7.101E-05	13.4700	Down
80		397.19	191.02002	[M-H]-	2-Dehydro-3-deoxy-D-glucarate	C6H8O7	C03921	49	1.6865	0.0004511	0.2047	Up
81		328.20	183.05099	[M]+	4-Pyridoxic acid	C8H9NO4	C00847	17	1.6697	0.0003729	0.4373	Up
82		83.71	209.02964	[M-H]-	Galactaric acid	C6H10O8	C00879	49	1.4517	0.0041889	1.5491	Down
83		746.26	583.25244	[M+H]+	Biliverdin	C33H34N4O6	C00500	36	1.3440	0.0077015	0.3850	Up
84		208.94	240.10835	[M+H]+	Dihydrobiopterin	C9H13N5O3	C02953	37	1.2961	0.0107908	0.5629	Up
85		90.24	189.15935	[M+H]+	7,8-Diaminononanoate	C9H20N2O2	C01037	41	1.2250	0.0171781	0.3611	Up
86		371.12	220.11757	[M+H]+	Pantothenic acid	C9H17NO5	C00864	20, 30	1.1355	0.0291618	0.7327	Up
87		405.28	413.13859	[M]+	6-Amino-6-deoxyfutalosine	C19H19N5O6	C20773	21	1.1222	0.0313913	0.4525	Up
88	Energy	723.67	251.12682	[M+H]+	Ubiquinone-1	C14H18O4	C00399	39	1.2849	0.0116498	0.2111	Up

(*Continued*)

Table I (Continued).

No.		RT	m/z	Mode	Metabolites	Formula	KEGG	Pathway	VIP	P	Fold Change CTRL/LPS	Tendency in Model Samples
89	Lipid	813.99	335.22378	[M-H]-	Hepoxilin B3	C20H32O4	C14810	12	2.0555	8.292E-07	6.1510	Down
90		606.61	465.30538	[M]-	Glycocholic acid	C26H43NO6	C01921	46	1.9985	3.318E-06	14.3250	Down
91		833.89	317.2122	[M-H]-	5-KETE	C20H30O3	C14732	12	1.8617	4.318E-05	5.2469	Down
92		93.66	102.95519	[M-H]-	Malonate	C3H4O4	C00383	16, 30, 44	1.8564	4.696E-05	0.7676	Up
93		606.94	335.2211	[M+H]+	12-Keto-leukotriene B4	C20H30O4	C05949	12	1.8505	2.832E-05	4.7623	Down
94		85.48	171.00529	[M-H]-	Glycerophosphoric acid	C3H9O6P	C00093	27, 42	1.7947	0.0001164	0.5785	Up
95		818.82	378.2431	[M-H]-	Sphingosine 1-phosphate	C18H38NO5P	C06124	27	1.7132	0.0003308	1.5492	Down
96		34.39	148.97762	[M+H]+	L-2-Hydroxyglutaric acid	C5H8O5	C03196	35	1.7110	0.0002237	0.9318	Up
97		732.19	313.23964	[M-H]-	9,10-DHOA	C18H34O4	C14828	34	1.6171	0.0009503	1.8629	Down
98		787.12	279.23352	[M-H]-	Rumenic acid	C18H32O2	C04056	34	1.5916	0.0012235	0.5072	Up
99		830.10	382.27236	[M+H]+	Sphinganine 1-phosphate	C18H40NO5P	C01120	27	1.5260	0.0017061	1.5645	Down
100		557.52	369.22838	[M-H]-	Thromboxane B2	C20H34O6	C05963	12	1.4837	0.0032286	2.5713	Down
101		815.19	387.19463	[M+H]+	Cholesterol	C27H46O	C00187	31, 38, 46	1.4589	0.003114	0.7189	Up
102		858.53	317.21005	[M+H-H₂O]+	Delta-12-Prostaglandin J2	C20H30O4	C05958	12	1.4140	0.0045121	0.0882	Up
103		753.98	295.22596	[M+H-H₂O]+	13(S)-HPOD	C18H32O4	C04717	34	1.3934	0.0053104	0.9383	Up
104		675.90	369.22353	[M+H]+	11-Dehydro-thromboxane B2	C20H32O6	C05964	12	1.3150	0.0094714	1.2263	Down
105		622.55	363.21553	[M+H]+	18-Hydroxycorticosterone	C21H30O5	C01124	38	1.2890	0.0113286	0.1270	Up
106		723.59	371.25644	[M+H]+	6-Keto-prostaglandin F1a	C20H34O6	C05961	12	1.2567	0.0140377	0.1709	Up
107		70.81	88.076036	[M]+	Butyric acid	C4H8O2	C00246	11	1.2438	0.0152528	1.4739	Down
108		464.75	445.18972	[M-H]-	Estrone glucuronide	C24H30O8	C11133	38	1.2126	0.0214229	0.3373	Up
109		101.65	146.11687	[M+H]+	Acetylcholine	C7H16NO2	C01996	42	1.1982	0.0202529	0.6468	Up
110		833.84	279.23355	[M-H]-	Linoleic acid	C18H32O2	C01595	34	1.1799	0.0258432	0.5599	Up
111		828.90	295.22808	[M-H]-	9(10)-EpOME	C18H32O3	C14825	34	1.1503	0.0304467	1.4408	Down
112		857.49	221.18957	[M+H]+	2-trans,6-trans-Farnesal	C15H24O	C03461	19	1.1469	0.0273532	0.7329	Up
113		670.16	448.30825	[M-H]-	Glycochenodeoxycholic acid	C26H43NO5	C05466	46	1.0824	0.0434284	7.9206	Down
114		421.39	283.17422	[M+H]+	Oleic acid	C18H34O2	C00712	44	1.0479	0.0464643	0.8811	Up

115	Nucleotide	107.58	283.06836	[M-H]-	Xanthosine	C10H12N4O6	C01762	2	2.1222	1.121E-07	6.4458	Down
116		331.25	153.04041	[M+H]+	Xanthine	C5H4N4O2	C00385	2	2.0620	2.084E-07	5.9132	Down
117		214.95	243.06182	[M-H]-	Uridine	C9H12N2O6	C00299	16	1.9477	9.548E-06	3.3624	Down
118		288.21	268.10346	[M+H]+	Adenosine	C10H13N5O4	C00212	2	1.6969	0.0002674	2.0077	Down
119		153.21	228.09663	[M+H]+	Deoxycytidine	C9H13N3O4	C00881	16	1.6858	0.0003071	0.7351	Up
120		106.59	112.05117	[M+H]+	Cytosine	C4H5N3O	C00380	16	1.4547	0.0032268	0.8241	Up
121		320.66	134.04521	[M-H]-	Adenine	C5H5N5	C00147	2	1.4489	0.0042826	2.8024	Down
122		294.35	115.03875	[M+H]+	Dihydrouracil	C4H6N2O2	C00429	16, 20, 30	1.4191	0.0043329	0.4377	Up
123		182.23	135.0284	[M-H]-	Hypoxanthine	C5H4N4O	C00262	2	1.3132	0.0114433	0.2934	Up
124		77.05	125.98603	[M]+	Thymine	C5H6N2O2	C00178	16	1.2065	0.0192534	2.5736	Down
125		106.34	244.09162	[M+H]+	Cytidine	C9H13N3O5	C00475	16	1.1554	0.0260572	1.4451	Down
126		157.06	243.0618	[M-H]-	Pseudouridine	C9H12N2O6	C02067	16	1.0540	0.0499762	0.6966	Up
127	Peptide	831.64	250.11792	[M]+	Gamma-Glutamylcysteine	C8H14N2O5S	C00669	4	1.2754	0.0124114	1.4233	Down

Notes: Pathway name: 1 alanine, aspartate and glutamate metabolism; 2 purine metabolism; 3 cysteine and methionine metabolism; 4 glutathione metabolism; 5 phenylalanine, tyrosine and tryptophan biosynthesis; 6 citrate cycle (TCA cycle); 7 arginine and proline metabolism; 8 lysine biosynthesis; 9 phenylalanine metabolism; 10 pentose phosphate pathway; 11 butanoate metabolism; 12 arachidonic acid metabolism; 13 tryptophan metabolism; 14 pyruvate metabolism; 15 hydroxy fatty acids; 16 pyrimidine metabolism; 17 vitamin B6 metabolism; 18 propanoate metabolism; 19 terpenoid backbone biosynthesis; 20 pantothenate and CoA biosynthesis; 21 ubiquinone and other terpenoid-quinone biosynthesis; 22 glycine, serine and threonine metabolism; 23 tyrosine metabolism; 24 fructose and mannose metabolism; 25 saturated fatty acids; 26 valine, leucine and isoleucine biosynthesis; 27 sphingoLipid; 28 histidine metabolism; 29 D-arginine and D-ornithine metabolism; 30 beta-alanine metabolism; 31 steroid biosynthesis; 32 glyoxylate and dicarboxylate metabolism; 33 D-glutamine and D-glutamate metabolism; 34 linoleic acid metabolism; 35 lysine degradation; 36 porphyrin and chlorophyll metabolism; 37 folate biosynthesis; 38 steroid hormone biosynthesis; 39 oxidative phosphorylation; 40 gamma-glutamyl amino acid; 41 biotin metabolism; 42 glycerophosphoLipid; 43 valine, leucine and isoleucine degradation; 44 fatty acid biosynthesis; 45 starch and sucrose metabolism; 46 primary bile acid biosynthesis; 47 arginine biosynthesis; 48 galactose metabolism; 49 ascorbate and aldarate metabolism; 50 taurine and hypotaurine metabolism; 51 amino sugar and nucleotide sugar metabolism; 52 pentose and glucuronate interconversions; 53 primary bile acid biosynthesis.
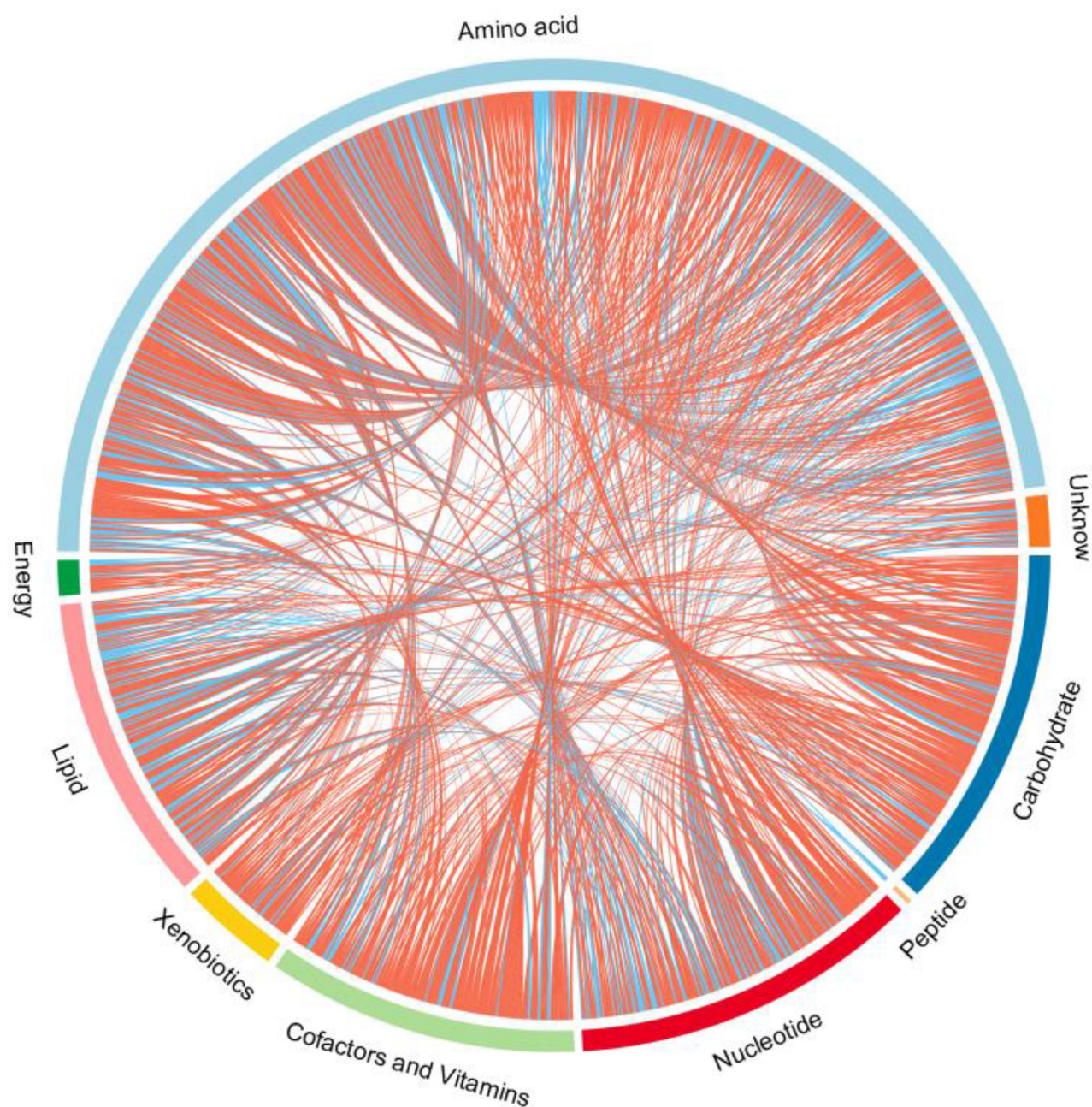
Figure 6 Chord diagram of differential serum metabolites. Classification of the metabolites detected into major functional classes.

(Figure 7A). As shown in Figure 7B, the interactions among the pathways mainly relate to amino acid and carbohydrate metabolism. Regarding the points, the size represents the pathway impact value and the color represents the degree of pathway correlation (based on the number of connected nodes).

The results of the correlation analysis indicated the possible interactions between the metabolic pathways affected by LPS (Figure 8). The possible interactions between the candidate biomarkers and pathways were determined based on metabolites with altered abundance between the LPS and control groups and an analysis using the KEGG database.

Discussion

LPS, an integral component of the Gram-negative bacterial outer membrane, can cause an uncontrollable inflammatory response, which can lead to damage to liver, kidney, lung and, eventually, fatal sepsis syndrome.[19] Thus, LPS was the classic inducer to establish multiple inflammatory
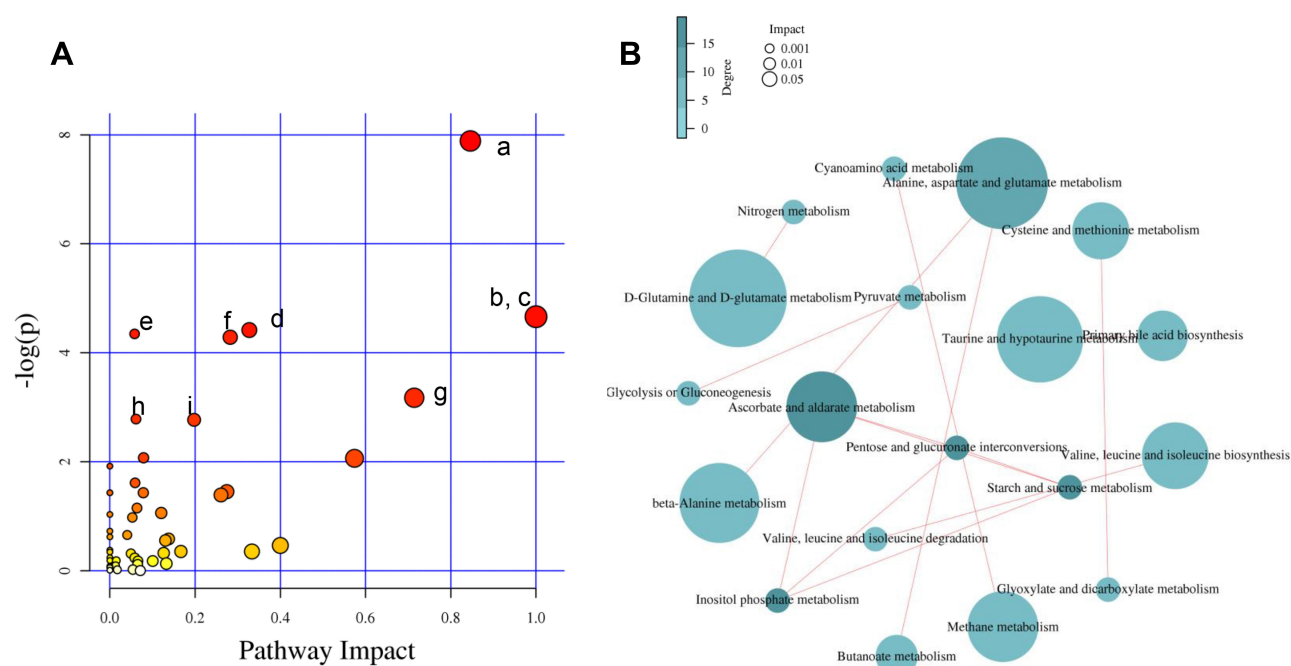
Figure 7 Pathway analysis. (**A**) Summary of pathway analysis. (a) Alanine, aspartate, and glutamate metabolism; (b) D-glutamine and D-glutamate metabolism; (c) linoleic acid metabolism; (d) arginine and proline metabolism; (e) butanoate metabolism; (f) glutathione metabolism; (g) taurine and hypotaurine metabolism; (h) pantothenate and coenzyme A (CoA) biosynthesis and (i) cysteine and methionine metabolism. Log (P) values from the pathway enrichment analysis are shown on the *y*-axis, and pathway impact values from the pathway topology analysis are shown on the *x*-axis. (**B**) Network diagram of metabolic pathway. The size represents the pathway impact value and the color represents the degree of pathway correlation (based on the number of connected nodes).

disease models. However, more evidences indicated that the mechanism that causes inflammation response is not just related to cytokine release. It is necessary to comprehensively understand LPS-induced liver and kidney injury based on metabolomics.

As compared to NMR, GC-MS and LC-MS are more sensitive and automated, which are better suited for the measurement of low-abundant metabolites and a variety of classes of compounds. Furthermore, GC-MS is more suitable for the analysis of volatile or thermally stable substance, including organic acids, amino acids, sugars and fatty acids, etc.[20] However, LC-MS is widely used for "untargeted" metabolomics because it effectively detects a broad range of different types, especially for unstable or non-volatility metabolites.[7] Related researches have reported the metabolomics changes in rats with LPS-induced systemic inflammatory response by GC-MS in lower doses which has shown that about 24 metabolites were differentially in the serum and mainly related to aminoacyl-tRNA biosynthesis, glutathione metabolism and arginine biosynthesis.[18] In this study, more metabolomics and regulatory pathways were detected and analyzed by LC-MS to comprehensively explain the pathogenesis of LPS-induced kidney and liver damage. In addition,

different treatment concentration or period of LPS lead to multiple disease symptoms, and this might be related to different metabolic response. Thus, this study focused on the mechanism and changes of acute kidney and liver injury induced by LPS in high-dose (10 mg/kg).

In this study, the systemic inflammatory tissue damage, biochemical indexes, and altered metabolic pathways were examined by histopathological evaluation, molecular biological methods, and LC-MS, respectively. Histopathological damage to the organs including the kidneys, liver, colon, and lungs occurred within 8 h after LPS was injected intraperitoneally. There were also significant changes in blood counts (WBC, monocyte, neutrophil, and lymphocyte counts), inflammatory factors (TNF-α and IL-6), oxidative stress indexes (SOD, MDA, and CAT activity), renal function indexes (serum +Cr and BUN), and liver function indexes (ALT, AST, and TBA). In the metabolomics analysis, 127 metabolites with altered abundance were identified; based on this, 53 pathways were identified as relevant to the pathological process, mainly involving the metabolism of D-glutamine and D-glutamate, linoleic acid, taurine and hypotaurine, beta-alanine, glutathione, and butanoate. The altered pathways are involved in multiple
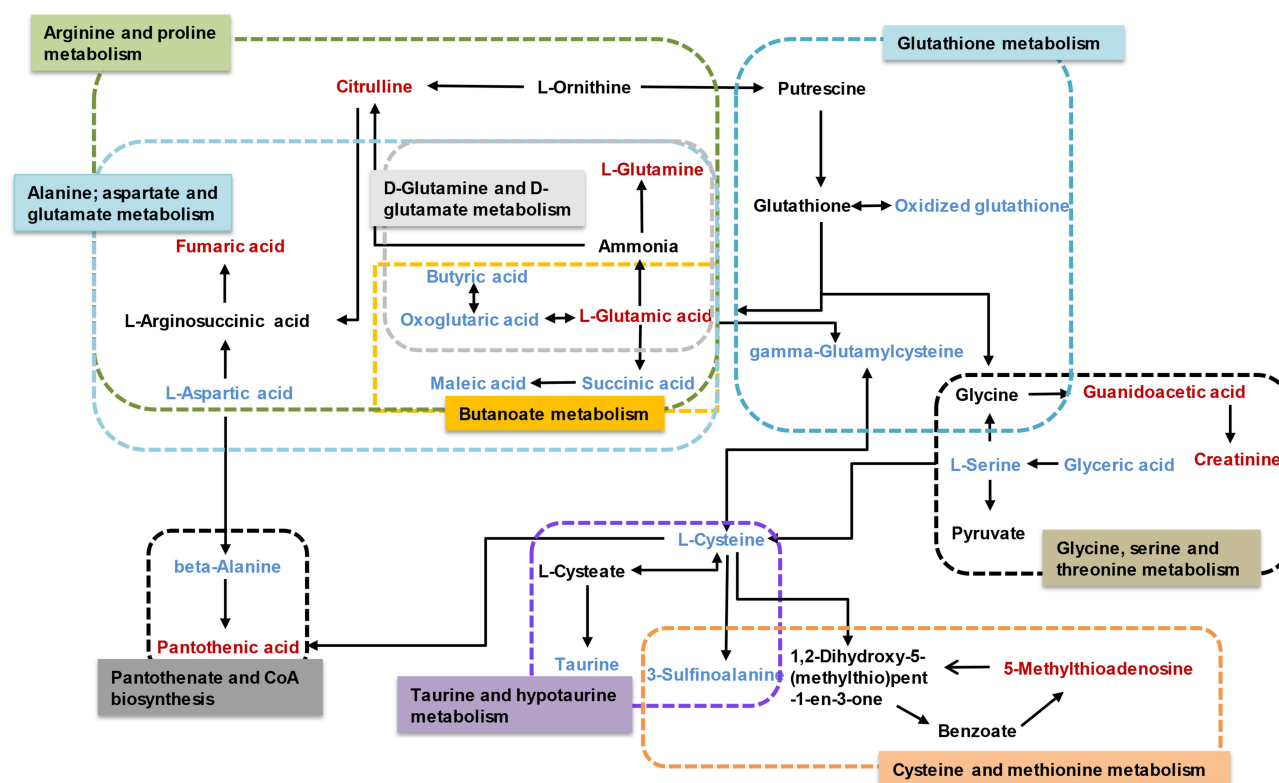
Figure 8 Schematic diagram of the disturbed metabolic pathways affected by LPS. Red indicates increased abundance and blue indicates decreased abundance in the LPS group compared to the control group.

physiological processes, including the inflammatory response, oxidative stress, energy metabolism, and amino acid metabolism.

Inflammatory Response

Regarding lipids, there were significant alterations in the levels of oleic acid, linoleic acid, and arachidonic acid-related metabolites. Linoleic acid is a precursor of arachidonic acid, which can be converted into various lipid mediators involved in the regulation of immunity.[21] Linoleic acid metabolism, arachidonic acid metabolism, and prostaglandin-related metabolites (delta-12-prostaglandin J2 and 6-keto-prostaglandin F1a) were significantly altered in the LPS group, which is consistent with previous research.[22] Oleic acid has been demonstrated to promote wound healing, combat autoimmune conditions, and eliminate pathogens by affecting macrophages, lymphocytes, and neutrophils.[23] The increase in oleic acid suggested that it might represent a self-protection mechanism in the acute inflammatory stage after LPS treatment for 8 h.

Glycocholic acid, a bile acid related to liver function, effectively inhibits both acute and chronic inflammation.[24]

There was a marked reduction in glycocholic acid, which is consistent with the occurrence of liver injury.

D-Glutamine and D-glutamate metabolism are associated with cell growth, lipid peroxidation, antioxidant defense, and anti-inflammation.[25,26] Glutamine is a principal biosynthesis material, contributing to nucleotide and nonessential amino acid synthesis.[27] Glutamine increases glutathione synthesis and alleviates renal dysfunction, liver fibrosis and inflammatory cytokine production.[28–30] Supplementing with glutamine reduces pulmonary functional and morphological impairment and inflammation in acute respiratory distress syndrome (ARDS).[31] There was a notable increase in glutamine after LPS administration, while no increases were found in glutathione, glutamate, or related amino acids, indicating that the body tried to modulate the anti-inflammatory response during the organ damage.

Oxidative Stress

LPS could induce the reactive oxygen species (ROS) accumulation, then decrease antioxidant defenses and lipid peroxidation of biological membranes with increased MDA production, which finally aggravates liver and

kidney injury and in turn results in many pathological changes. Oxidative stress not only causes a series of morphological changes such as vacuolar degeneration, apoptosis, inflammatory cell infiltration and necrosis of renal parenchymal cells and hepatocytes, but also reduces glomerular filtration function and renal tubule reabsorption function. In present study, several biochemical parameters were assessed to determine the level of oxidative stress damage, including MDA, SOD and CAT activities. MDA is a representative product of polyunsaturated fatty acid peroxidation, which can be increased by oxidative stress.[32] Hydroxyl radical and ROS are dismutated by SOD to generate hydrogen peroxide, which can be decomposed by CAT.[33] The MDA level was significantly increased in the LPS group, while the activities of SOD and CAT were markedly decreased, indicating oxidative stress damage.

Taurine and hypotaurine metabolism, glycine metabolism, cysteine and methionine metabolism, pantothenate and coenzyme A (CoA) biosynthesis and glutathione metabolism are associated with antioxidant defense and anti-lipid peroxidation. The liver is the predominant place to secret bile, and any changes of bile acid homeostasis were linked to various types of liver injury. Taurine is well known as an abundant amino that possesses various physiological functions, such as bile acid conjugation, osmoregulation, and detoxification.[34] Taurine and betaine both play important roles in scavenging ROS and improving antioxidant status and attenuating apoptosis and necrosis in LPS-induced liver injury.[35–38] In this study, LPS induced pathological damage and increased the ALT/AST and TBA levels, and it dramatically decreased the serum levels of taurine and betaine aldehyde (which can be transformed into betaine), which might be a self-protection mechanism to attenuate LPS-induced oxidative damage. Cysteine, as the key critical precursor of glutathione synthesis, can scavenge and combine with free radicals. L-cysteine and L-cystine are transformed into one another based on the redox state of the cell.[39] In this study, the level of L-cystine was higher while the level of L-cysteine was lower in the LPS group than the control group, indicating a disturbance of redox homeostasis after LPS administration and concurring with previous research.[40] Glutathione metabolism helps maintain the normal function of liver and kidney,[41] and glutathione metabolism was down-regulated in the LPS group, with the significant changes in oxidized glutathione and L-glutamine.

Pantothenic acid is the precursor of coenzyme A (CoA), which participates in sugar, lipid, and protein metabolism, suggesting an anti-lipid peroxidation effect. The possible regulatory mechanisms include scavenging ROS to protect cell membrane integrity, promoting phospholipid synthesis for repair, and increasing glutathione biosynthesis.[40] Elevated pantothenic acid may be a protective response after LPS treatment.

Amino Acid Metabolism

The metabolomics results showed that the levels of multiple branched-chain amino acids (BCAAs) were significantly decreased in the LPS group compared to the control group, indicating a lack of energy and biological materials. As the metabolomics results showed that the serum levels of several amino acids were disturbed in the LPS group, LPS-induced acute liver and kidney injury were clearly associated with the alterations in amino acid metabolism (Table 1). The levels of glutamic acid, aspartic acid, proline, serine, alanine, tyrosine, cysteine, and isoleucine were decreased after LPS administration, which was related to the down-regulation of alanine, aspartate, and glutamate metabolism, arginine and proline metabolism, and cysteine and methionine metabolism. Essential amino acids play critical roles in regulating energy metabolism and synthesizing proteins of the body.[42] In the study, serine and glycine were reduced, which are the potent antioxidants to scavenge free radicals and play a key role in anti-oxidative defense of liver cell.[43] The decreased tyrosine level in the LPS group indicated LPS-induced kidney injury, as decreased tyrosine has been observed in chronic renal damage.[44] Arginine is suggested as a potential biomarker in hepatic and renal injuries and served as a precursor for BUN and Cr.[45] The increased level of BUN and Cr and arginine-related metabolites in LPS group indicated a disturbance of arginine metabolism. In addition, LPS-induced renal injury could be evidenced by the decreased level of tyrosine, which has been reported in chronic renal damage.[42] Glutamic acid, as a key amino acid, serves as a signaling factor between the immune and nervous systems, a key transamination partner required for glutathione regulation, and a critical component of the defense against oxidative stress.[43,46] The reduction in glutamic acid in the LPS group may indicate the damage due to inflammatory cytokines and ROS. Above alterations have been shown to induce oxidative stress and enhance amino acid catabolism, which might further aggravate the

pathological damage and disturb normal biological function.[43,47]

Conclusion

In this study, multiple methods were used to investigate the pathological characteristics and changes in biochemical indexes during LPS-induced acute systemic inflammation. An untargeted metabolomics method involving UPLC-QTOF/MS was used to analyze the metabolite profile. In the acute systemic inflammation model, pathological injury occurred in the liver, colon, lungs, and kidneys. LPS significantly altered the serum levels of 127 metabolites, which were found to be involved in 53 pathways. The 10 most relevant pathways (Figure 8) were found to involve amino acid metabolism and lipid metabolism, and these were identified by the KEGG analysis as being involved in the regulation of multiple physiological processes, including the inflammatory response, oxidative stress, and amino acid metabolism. The results suggested that LPS-induced acute systemic inflammation mainly involves the inflammatory response, oxidative stress, and protein synthesis, causing organ damage and functional impairment. The differential metabolites and metabolic pathways identified in this paper should be further studied using targeted metabolomics, lipidomics, and proteomics, in order to elucidate mechanisms and screening therapeutic targets for developing early diagnostic strategies and treatments.

Acknowledgments

Disclosure

The authors report no conflicts of interest.

References

1. Deng M, Scott MJ, Loughran P, et al. Lipopolysaccharide clearance, bacterial clearance, and systemic inflammatory responses are regulated by cell type-specific functions of TLR4 during sepsis. *J Immunol*. 2013;190(10):5152–5160. doi:10.4049/jimmunol.1300496
2. Calvano SE, Coyle SM. Experimental human endotoxemia: a model of the systemic inflammatory response syndrome? *Surg Infect (Larchmt)*. 2012;13(5):293–299. doi:10.1089/sur.2012.155
3. Fong YM, Marano MA, Moldawer LL, et al. The acute splanchnic and peripheral tissue metabolic response to endotoxin in humans. *J Clin Invest*. 1990;85(6):1896–1904. doi:10.1172/JCI114651
4. Khovidhunkit W, Kim MS, Memon RA, et al. Effects of infection and inflammation on lipid and lipoprotein metabolism: mechanisms and consequences to the host. *J Lipid Res*. 2004;45(7):1169–1196.

5. Pearce EL, Pearce EJ. Metabolic pathways in immune cell activation and quiescence. *Immunity*. 2013;38(4):633–643. doi:10.1016/j.immuni.2013.04.005
6. Schrimpe-Rutledge AC, Codreanu SG, Sherrod SD, et al. Untargeted metabolomics strategies-challenges and emerging directions. *J Am Soc Mass Spectrom*. 2016;27(12):1897–1905. doi:10.1007/s13361-016-1469-y
7. Eckerle M, Ambroggio L, Puskarich M, et al. Metabolomics as a driver in advancing precision medicine in sepsis. *Pharmacotherapy*. 2017;37(9):1023–1032. doi:10.1002/phar.1974
8. Zhang H, Sha J, Feng X, et al. Dexmedetomidine ameliorates LPS induced acute lung injury via GSK-3β/STAT3-NF-κB signaling pathway in rats. *Int Immunopharmacol*. 2019;74:105717. doi:10.1016/j.intimp.2019.105717
9. Abdelmageed M, El-Awady M, Suddek G. Apocynin ameliorates endotoxin-induced acute lung injury in rats. *Int Immunopharmacol*. 2016;30:163–170. doi:10.1016/j.intimp.2015.12.006
10. Dunn WB, Broadhurst D, Begley P, et al. Procedures for large-scale metabolic profiling of serum and plasma using gas chromatography and liquid chromatography coupled to mass spectrometry. *Nat Protoc*. 2011;6(7):1060–1083. doi:10.1038/nprot.2011.335
11. Zelena E, Dunn WB, Broadhurst D, et al. Development of a robust and repeatable UPLC-MS method for the long-term metabolomic study of human serum. *Anal Chem*. 2009;81(4):1357–1364. doi:10.1021/ac8019366
12. Want EJ, Masson P, Michopoulos F, et al. Global metabolic profiling of animal and human tissues via UPLC-MS. *Nat Protoc*. 2013;8(1):17–32. doi:10.1038/nprot.2012.135
13. Liu M, Gong X, Quan Y, et al. A cell-based metabonomics approach to investigate the varied influences of chrysophanol-8-O-β-D-glucoside with different concentrations on L-02 cells. *Front Pharmacol*. 2018;9:1530. doi:10.3389/fphar.2018.01530
14. Thevenot EA, Roux A, Xu Y, et al. Analysis of the human adult urinary metabolome variations with age, body mass index, and gender by implementing a comprehensive workflow for univariate and OPLS statistical analyses. *J Proteome Res*. 2015;14(8):3322–3335. doi:10.1021/acs.jproteome.5b00354
15. Huang X, Gan G, Wang X, et al. The HGF-MET axis coordinates liver cancer metabolism and autophagy for chemotherapeutic resistance. *Autophagy*. 2019;15(7):1258–1279. doi:10.1080/15548627.2019.1580105
16. Kasawara KT, Cotechini T, Macdonald-Goodfellow SK, et al. Moderate exercise attenuates lipopolysaccharide-induced inflammation and associated maternal and fetal morbidities in pregnant rats. *PLoS One*. 2016;11(4):e0154405. doi:10.1371/journal.pone.0154405
17. Shan J, Qian W, Kang A, et al. Lipid profile perturbations in the plasma and lungs of mice with LPS-induced acute lung injury revealed by UHPLC-ESI-Q exactive HF MS analysis. *J Pharm Biomed Anal*. 2019;162:242–248. doi:10.1016/j.jpba.2018.09.037
18. Geng C, Guo Y, Wang C, et al. Comprehensive evaluation of lipopolysaccharide-induced changes in rats based on metabolomics. *J Inflamm Res*. 2020;13:477–486. doi:10.2147/JIR.S266012
19. Seán TA, Seán C, Paul NM, et al. Lipopolysaccharide-induced sepsis induces long-lasting affective changes in the mouse. *Brain Behav Immun*. 2015;43:98–109. doi:10.1016/j.bbi.2014.07.007
20. Zeki ÖC, Eylem CC, Reçber T, et al. Integration of GC-MS and LC-MS for untargeted metabolomics profiling. *J Pharm Biomed Anal*. 2020;190:113509. doi:10.1016/j.jpba.2020.113509
21. Ameer YT, Helene CB, Yewon C, et al. Dietary linoleic acid lowering reduces lipopolysaccharide-induced increase in brain arachidonic acid metabolism. *Mol Neurobiol*. 2017;54(6):4303–4315. doi:10.1007/s12035-016-9968-1

22. Liu YJ, Li H, Tian Y, et al. PCTR1 ameliorates lipopolysaccharide-induced acute inflammation and multiple organ damage via regulation of linoleic acid metabolism by promoting FADS1/FASDS2/ELOV2 expression and reducing PLA2 expression. *Lab Invest*. 2020;100(7):904–915. doi:10.1038/s41374-020-0412-9

23. Helioswilton SC, Patrícia RS, Bethânea CP, da Silva JS, Cardoso CR. An overview of the modulatory effects of oleic acid in health and disease. *Mini Rev Med Chem*. 2013;13(2):201–210.

24. Zohreh S, Kashaf R, Daniel RK, et al. Potential role of uric acid in metabolic syndrome, hypertension, kidney injury, and cardiovascular diseases: is it time for reappraisal? *Curr Hypertens Rep*. 2013;15(3):175–181. doi:10.1007/s11906-013-0344-5

25. Minjiang C, Siming L, Hong Z, et al. Identification of the potential metabolic pathways involved in the hepatic tumorigenesis of rat diethylnitrosamine-induced hepatocellular carcinoma via H NMR-based metabolomic analysis. *Biomed Res Int*. 2019;9367082.

26. Qu XY, Gao H, Sun JM, et al. Identification of key metabolites during cisplatin-induced acute kidney injury using an HPLC-TOF/MS-based non-targeted urine and kidney metabolomics approach in rats. *Toxicology*. 2020;431:152366. doi:10.1016/j.tox.2020.152366

27. Zhu Y, Li TT, Suzane RS, et al. A critical role of glutamine and asparagine γ-nitrogen in nucleotide biosynthesis in cancer cells hijacked by an oncogenic virus. *MBio*. 2017;8(4):e01179–17. doi:10.1128/mBio.01179-17

28. Zhang F, Wang XY, Pan LY, et al. Glutamine attenuates lipopolysaccharide-induced acute lung injury. *Nutrition*. 2009;25(6):692–698. doi:10.1016/j.nut.2008.11.032

29. Shrestha N, Chand L, Han M, et al. Glutamine inhibits CCl4 induced liver fibrosis in mice and TGF-β1 mediated epithelial-mesenchymal transition in mouse hepatocytes. *Food Chem Toxicol*. 2016;93:129–137. doi:10.1016/j.fct.2016.04.024

30. Zhan F, Wang X, Zhang J, et al. Glutamine alleviates the renal dysfunction associated with gentamicin-induced acute kidney injury in Sprague-Dawley rats. *Biotechnol Appl Biochem*. 2021;18.

31. Gisele PO, Jamil ZK, Phillipe SLG, et al. Glutamine therapy reduces inflammation and extracellular trap release in experimental acute respiratory distress syndrome of pulmonary origin. *Nutrients*. 2019;11(4):831. doi:10.3390/nu11040831

32. Inas AA, Mariam Y, Laila R, Solieman A. Lipid peroxidation plasma biomarker correlated with hepatic fibrosis in human Schistosoma mansoni infection. *Acta Parasitol*. 2015;60(4):735–742. doi:10.1515/ap-2015-0105

33. Li R, Zhou XQ, Liu D, et al. Enhancing the activity and stability of Mn-superoxide dismutase by one-by-one ligation to catalase. *Free Radic Biol Med*. 2018;129:138–145. doi:10.1016/j.freeradbiomed.2018.09.018

34. Wu Q, Zhang H, Dong X, et al. UPLC-Q-TOF/MS based metabolomic profiling of serum and urine of hyperlipidemic rats induced by high fat diet. *J Pharm Anal*. 2014;4(6):360–367. doi:10.1016/j.jpha.2014.04.002

35. Kayoko S, Chian JJ, Kyoko T, et al. Role of ROS production and turnover in the antioxidant activity of taurine. *Adv Exp Med Biol*. 2015;803:581–596.

36. Shao HB, Chu LY, Lu ZH, et al. Primary antioxidant free radical scavenging and redox signaling pathways in higher plant cells. *Int J Biol Sci*. 2007;4(1):8–14. doi:10.7150/ijbs.4.8

37. Schaffer SW, Jong CJ, Ramila KC, et al. Physiological roles of taurine in heart and muscle. *J Biomed Sci*. 2010;17(Suppl 1):S2. doi:10.1186/1423-0127-17-S1-S2

38. Liu YY, Li F, Zhang L, et al. Taurine alleviates lipopolysaccharide-induced liver injury by anti-inflammation and antioxidants in rats. *Mol Med Rep*. 2017;16(5):6512–6517. doi:10.3892/mmr.2017.7414

39. Gordon FR, Ian LM. Existing and potential therapeutic uses for N-acetylcysteine: the need for conversion to intracellular glutathione for antioxidant benefits. *Pharmacol Ther*. 2014;141(2):150–159. doi:10.1016/j.pharmthera.2013.09.006

40. Ping F, Guo Y, Cao YM, et al. Metabolomics analysis of the renal cortex in rats with acute kidney injury induced by sepsis. *Front Mol Biosci*. 2019;6:152. doi:10.3389/fmolb.2019.00152

41. Homma T, Fujii J. Application of glutathione as anti-oxidative and anti-aging drugs. *Curr Drug Metab*. 2015;16(7):560–571. doi:10.2174/1389200216666151015114515

42. Liao ST, Li P, Wang JS, et al. Protection of baicalin against lipopolysaccharide induced liver and kidney injuries based on H NMR metabolomic profiling. *Toxicol Res*. 2016;5(4):1148–1159. doi:10.1039/C6TX00082G

43. Shi C, Han X, Mao X, et al. Metabolic profiling of liver tissues in mice after instillation of fine particulate matter. *Sci Total Environ*. 2019;696:133974. doi:10.1016/j.scitotenv.2019.133974

44. José MFC, Manfred WB, Milton F, et al. Maleylacetoacetate isomerase (MAAI/GSTZ)-deficient mice reveal a glutathione-dependent nonenzymatic bypass in tyrosine catabolism. *Mol Cell Biol*. 2002;22(13):4943–4951. doi:10.1128/MCB.22.13.4943-4951.2002

45. Saitoh W, Yamauchi S, Watanabe K, et al. Metabolomic analysis of arginine metabolism in acute hepatic injury in rats. *J Toxicol Sci*. 2014;39(1):41–50. doi:10.2131/jts.39.41

46. Yang CY, Hao RJ, Du XD, Wang Q, Deng Y, Sun R. Response to different dietary carbohydrate and protein levels of pearl oysters (Pinctada fucata martensii) as revealed by GC-TOF/MS-based metabolomics. *Sci Total Environ*. 2019;650:2614–2623. doi:10.1016/j.scitotenv.2018.10.023

47. Turner MC, Krewski D, Pope CA, et al. Long-term ambient fine particulate matter air pollution and lung cancer in a large cohort of never-smokers. *Am J Respir Crit Care Med*. 2011;184(12):1374–1381. doi:10.1164/rccm.201106-1011OC